ELSEVIER

Journal of Power Sources 106 (2002) 313–322

JOURNAL OF POWER SOURCES

www.elsevier.com/locate/jpowsour

Development of a compact 500 W class direct methanol fuel cell stack

H. Dohle*, H. Schmitz, T. Bewer, J. Mergel, D. Stolten

Institut fur Werkstoffe und Verfahren der Energietechnik, Forschungszentrum Jülich GmbH, D-52425 Jülich, Germany

Abstract

A 71-cell direct methanol fuel cell (DMFC) stack has been developed at Forschungszentrum Jülich. The system consists of the stack, a water/methanol tank, a heat exchanger, a pump and compressors as auxiliary components. The auxiliary components are driven by the DMFC stack itself without external power sources. The DMFC stack consists of 71 cells with an area of 144 cm^2. The current collectors are manufactured of stainless steel (1.4571) with a cell pitch (distance between two membrane electrode assemblies (MEAs)) of only 2 mm. The MEAs are fabricated in-house by a combination of a decal and direct coating method. The thickness of each current collector is 0.3 mm. Each cell is provided with effective flow fields for a homogeneous flow distribution. The flow distribution has been calculated and approved by experiments. Therefore, the necessary stoichiometric air flow rate is only in the range of 2–3. The air compressor is designed to supply air with a maximum pressure of 1.5 bar absolute to the cell.

Keywords: DMFC; Stack; System; Efficiency

1. Introduction

Direct methanol fuel cells (DMFCs) using polymer electrolyte membranes are promising candidates for portable power sources, electric vehicles and stationary applications because they do not require any fuel processing equipment and can be operated at low temperature. For the commercialisation of DMFCs, it is necessary to develop highly efficient cell component technology [1].

The Forschungszentrum Jülich demonstrated an air breathing 50 W stack at the Hannover Fair 2000 [2]. Optimization of both membrane electrode assemblies (MEAs) and stack design resulted in the development of a 500 W stack.

In a DMFC the following catalytically active reactions take place:

Anode:

$$CH_3OH + H_2O \Rightarrow CO_2 + 6H^+ + 6e^-$$

Cathode:

$$6H^+ + 6e^- + 1.5O_2 \Rightarrow 3H_2O$$

Overall reaction:

$$CH_3OH + 1.5O_2 \Rightarrow CO_2 + 2H_2O$$

The theoretical open circuit voltage can be calculated by dividing the free Gibbs reaction enthalpy ΔG by the number n of the electrons transferred during the reaction and the Faraday constant F:

$$U_o = \frac{\Delta G}{nF} \quad (1)$$

with $n = 6$, resulting in a theoretical open circuit voltage U_o of 1.21 V.

The cell potential during the operation is influenced towards lower voltages by ohmic losses, overvoltages at the electrodes and by the formation of a mixed potential at the cathode.

The cause of methanol permeation from the anode to the cathode is, on one hand, the diffusion of methanol. On the other hand, the protons carry methanol and water molecules by electro-osmosis from the anode to the cathode. The amount of methanol permeation depends on the operating conditions, especially on the methanol concentration and the current density [2]. The use of methanol as fuel is advantageous from the view of storage especially for portable power source applications. A DMFC stack of 45 cm^2 active area, designed for portable applications, has been reported recently by Ren et al. [3].

2. Stack assembling and component testing

The 500 W system consists of the stack, a water/methanol tank, a heat exchanger, a pump and compressors as auxiliary components. The DMFC stack consists of 71 cells with an area of 144 cm^2. The cell pitch (distance between the MEAs) is only 2 mm. This leads to a very compact stack design. The

* Corresponding author.

0378-7753/02/$ – see front matter
PII: S0378-7753(01)01064-3

Table 1
Stack specifications

Number of cells	71
Single cell area	144 cm^2
Cell pitch	<2 mm
Stack	160 mm × 160 mm × 165 mm (4.2 l)
Temperature	70 °C
Design data	
Current	20.6 A
Voltage	24.3 V
Power	500 W
Power density	50 mW/cm^2
MEA	
Membrane	Nafion-115
Anode	3.9 mg $PtRu/cm^2$
Cathode	2.3 mg Pt/cm^2

small cell pitch is achieved by using highly effective flow fields and thin metal current collectors of 0.3 mm width. All parts of the cell hardware such as sealings, current collectors and flow distribution components are 2D-shaped with regard to a cheap manufacturing process using standard manufacturing processes, such as punching or cutting. The auxiliary components are driven by the DMFC stack itself without external power sources. The water/methanol solution is circulated using a pump. The air compressor is designed to supply air with a maximum pressure of 1.5 bar absolute to the stack. A heat exchanger serves to remove excessive heat from the system and to keep the stack at temperatures around 70 °C (for stack specifications, see Table 1). Initial testing of the cell hardware was done with a 3-cell short stack (Fig. 1(a)) before assembling the 71-cell stack (Fig. 2). Fig. 1(b) summarizes shortly the initial testing of the MEAs

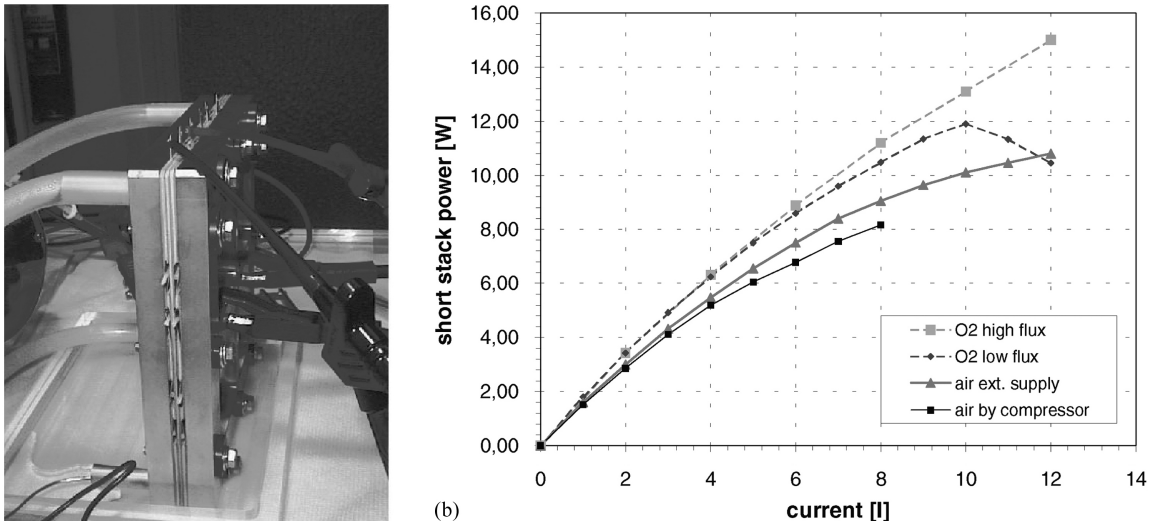

Fig. 1. (a) Photograph of the 3-cell short stack; (b) initial testing of the 3-cell short stack at various operating conditions at 45 °C. The current indicated in the picture is the net current, defined as the current produced by the stack less the current demand of the air compressor.

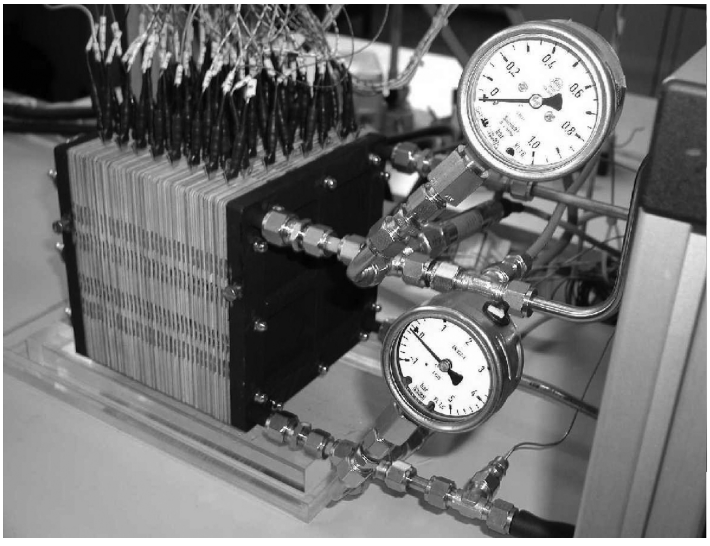

Fig. 2. Photograph of the 500 W DMFC stack.

mounted into the 3-cell short stack for operation with air and oxygen at a low temperature (45 °C). In other test equipments we tested the main components of the stack separately.

3. Fabrication of the membrane electrode assemblies

The MEA consists of a polymer membrane, anode and cathode catalyst layers and gas diffusion layers.

The MEAs mounted in the 500 W stack were fabricated in-house. We used Nafion-115 as membrane material. The anodic catalyst loading is 3.9 mg/cm^2 PtRu-black with an atomic ratio of 1:1, cathodic loadings are 2.3 mg/cm^2 Pt-black. The anode catalyst layer was prepared by a decal method, whereas the cathode was prepared by direct application of the catalysts to the membrane. The Nafion content of the anode catalyst layers has a great impact on the power density. On one hand, increasing the Nafion content increases the ionic conductivity of the catalyst layer, on

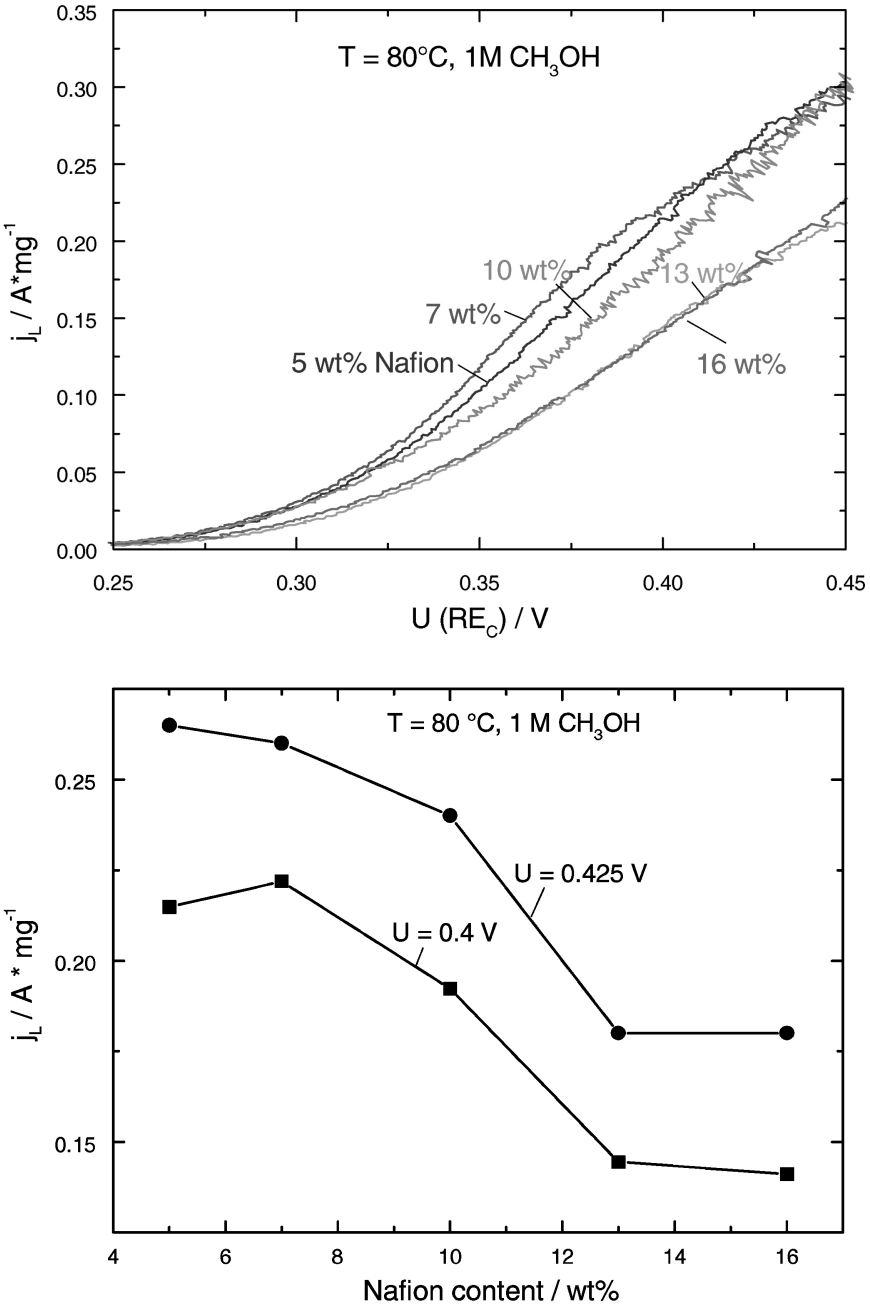

Fig. 3. Influence of the Nafion content in the anode catalyst layer on MeOH oxidation (PtRu) (top); influence of the Nafion content in the anode catalyst layer on current density at different anodic potentials (bottom). Data were obtained in half cell measurements vs. hydrogen.

the other hand, it reduces the mass transport of reactants. Therefore, we investigated the influence of the Nafion content in a range of 5–16 wt.% with regard to the electrochemical and structural properties [4]. The optimum Nafion content is 7 wt.%, showing the best performance (Fig. 3). This corresponds to the data of Gottesfeld et al. [5], who found optimal values of 6.5 wt.% for the anode and 10 wt.% for the cathode catalyst layer.

The anode gas diffusion layer was prepared by mixing carbon powder with finely-dispersed PTFE. Various PTFE contents were tested. The mixture was then applied to a carbon cloth with a loading of approx. 5 mg/cm^2 with a subsequent sintering process at 350 °C. For the optimization of the anode gas diffusion layer, we measured the anode power density for different PTFE contents.

The power density is not directly correlated to the PTFE content (Fig. 4). To find the parameters which influence the power density we investigated the structural parameters, in particular the fraction of hydrophobic and hydrophilic pores. The method to distinguish between hydrophobic and hydrophilic pores is based on the following steps: (1) filling the sample with water, which fills only the hydrophilic pores, (2) weighing, (3) drying, (4) weighing, (5) filling the sample with decane which fills both the hydrophilic and hydrophobic pores, and (6) weighing of the sample with filled pores.

The two weights depend on the amounts of both the hydrophobic and hydrophilic pores, and are used to calculate the different structural parameters. Details of the method are described in [4]. Current density strongly depends on the amount of hydrophobic pores with an increase by a factor of 2 from the lowest (51 vol.% at 16 wt.% PTFE) to the highest (84 vol.% at 13 wt.% PTFE) fraction of hydrophobic pores.

The cathode diffusion layer was graphite paper without any further treatment.

4. Current collectors

One important component of the stack is the current collector. The local contact resistance between the collector and the diffusion layer influences the current density distribution, as well as, the overall performance. The contact resistance is mainly a function of the local contact pressure and the local surface condition, i.e. grade of passivation, surface roughness, coatings, etc. In the following we briefly describe the newly developed method of measuring the contact resistance ex situ. Stainless steel and gold-plated stainless steel were investigated as current collectors. Two current collectors were inserted into a plastic frame with only one diffusion layer in between. Then a current was passed through the arrangement by means of an external current source.

The new method is based on the simultaneous measurement of the local heat radiation p_{heat} and the local voltage loss $\Delta U_{\text{contact}}$ due to the contact resistance R_{local} [6].

The local heat radiation depends on the current density i and the voltage loss $\Delta U_{\text{contact}}$ between the current collector and the diffusion layer:

$$p_{\text{heat}} = \Delta U_{\text{contact}} i$$

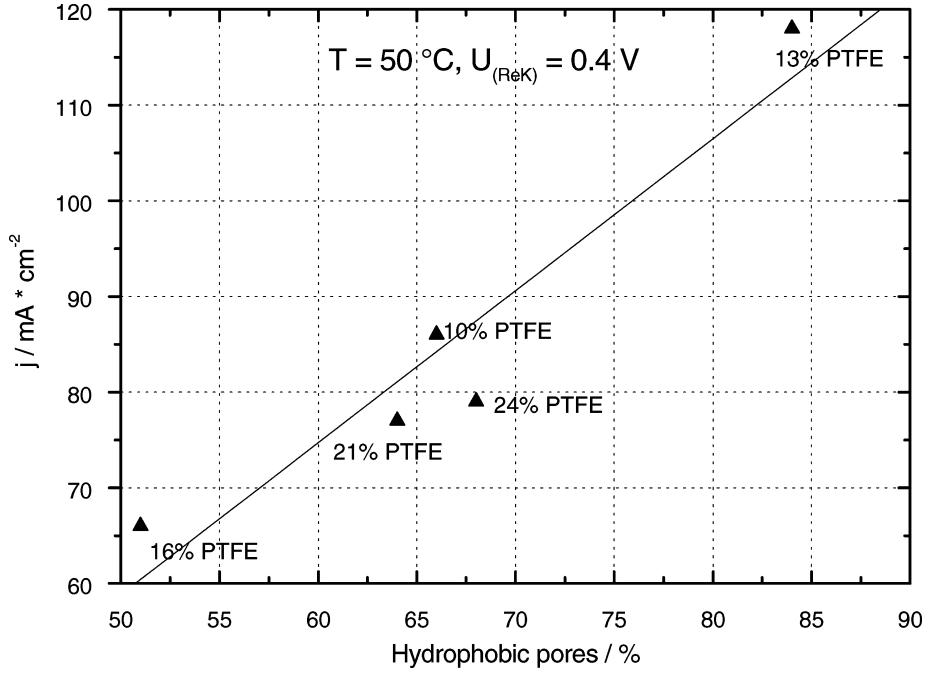

Fig. 4. Influence of PTFE content in the anode gas diffusion layer ($T = 50$ °C, $U = 0.4$ V); correlation of hydrophobic pore fraction and current density. The current density is not directly correlated to the PTFE content but to the fraction of hydrophobic pores [4].

with

$$i = \frac{\Delta U_{\text{contact}}}{R_{\text{local}}}$$

This leads to the expression

$$R_{\text{local}} = \frac{(\Delta U)^2_{\text{contact}}}{p_{\text{heat}}}$$

The local voltage loss between the current collector and the diffusion layer can be easily measured by contacting the two elements by a voltmeter. We used an infrared camera to measure the heat radiation. The gold-plated collectors have a very low and homogeneous contact resistance distribution compared to the stainless steel collectors. Fig. 5 briefly summarizes the results obtained from the combination of infrared measurements and potential measurements. It is shown that the ohmic resistance is reduced by two orders of magnitude due to gold-plating. Of course the ex situ measurements are not directly comparable to the in situ environment of a DMFC, but they can show the influence of material selection in a good approximation.

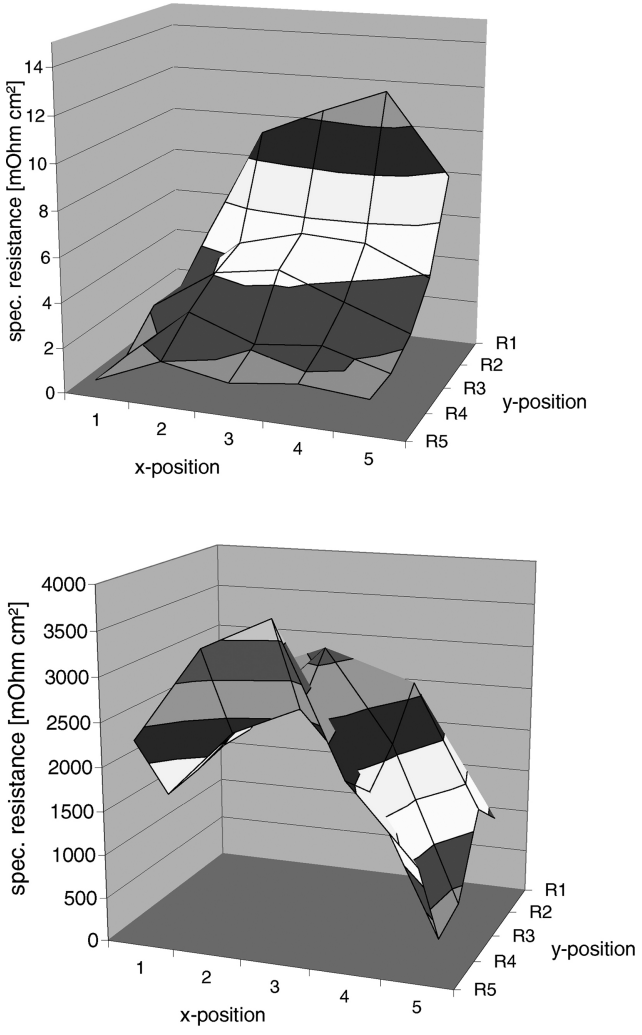

Fig. 5. Distribution of the specific contact resistance between the current collector and the diffusion layer (current collector: gold-plated stainless steel) (top); distribution of the specific contact resistance between the current collector and the diffusion layer (current collector: stainless steel) (bottom).

5. System and stack testing

The outer dimensions of the stack are 160 mm × 160 mm × 165 mm which corresponds to a total volume of 4.2 l. The weight of the stack is 12 kg. For the rather moderate operating conditions (ambient pressure, moderate temperature up to 80 °C) the power density is 120 W/l resp. 41 W/kg. In further work, this value will be increased by a combination of different approaches:

1. Increasing the power density by optimization of both the cathode catalyst layer and the gas diffusion layer structure.
2. Further optimization of the anode.
3. Reducing the fraction of the inactive volume of the stack such as sealings, screw holes, internal manifolds, etc.
4. Further reduction of the cell pitch due to smaller flow distribution structures.

An important issue in stack design is the optimal distribution of reactants towards the electrochemical active sites of each cell. In order to effectively utilize the entire area of the anode and cathode, as homogeneous a flow distribution as possible is required, so that the reactants are distributed homogeneously in the fuel cell. At the same time, the pressure loss should be as low as possible to minimize the energy requirements of the auxiliary units, such as pumps and compressors. The flow distribution for the flat flow distribution structure of the 500 W stack has been calculated and approved by experiments. Experiments used a special perspex test rig, which allows to inject dye using an injection pump to the water flow. The distribution can be observed visually. To simulate the conditions at the CO_2-evolving anodes, bubbles were supplied to the flow fields [7]. These experimental studies were supported by calculations using the computational fluid dynamics code FLUENT.

The chosen design showed very good distribution and bubble removal characteristics. The usage of these effective flow field on both the anode and the cathode enables us to reduce the necessary stoichiometric air flow rate to the range of 2–3. This low air flow results in a low parasitic power consumption of the air compressor, and therefore, in a higher net stack power. The homogeneity of power generation in the cells indicates an effective flow distribution also at low air flow rates. Fig. 6 shows measurements of the 3-cell stack for both air and oxygen operation at 45 °C. The power generation of each cell is rather homogeneous in air, as well as, in oxygen operation.

When using air, the air was not pre-heated and not humidified. Fig. 7 shows infrared photographs of the endplates

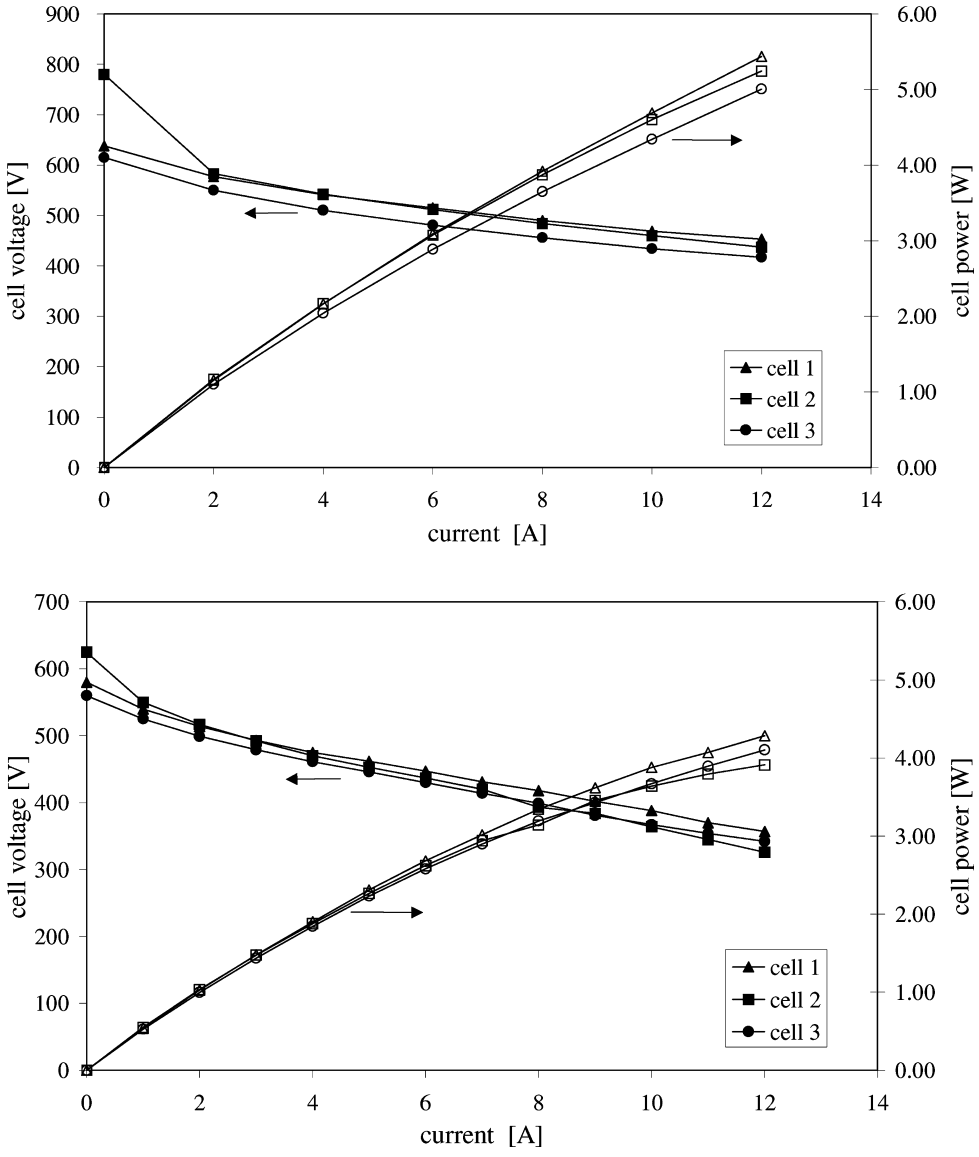

Fig. 6. Initial testing of the 3-cell short stack. The membrane electrode assemblies show homogeneous power output indicating a homogeneous flow distribution for operation on both oxygen (top) and air at ambient pressure (bottom). The temperature in both cases is 45 °C, the concentration of methanol is 1 M.

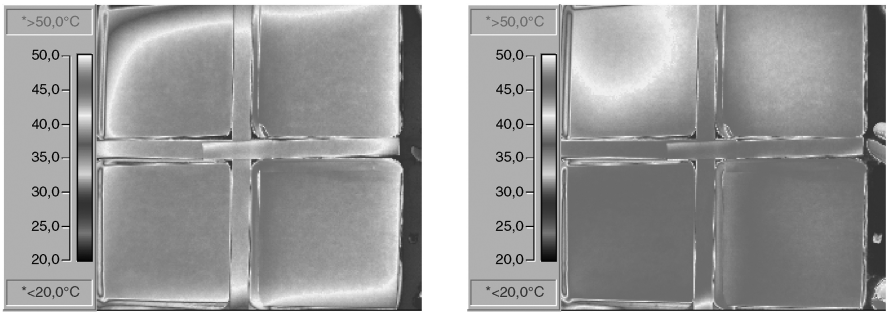

Fig. 7. Temperature distribution on the end plate of the stack for open circuit conditions (left) and 15 A current generation (right). The air inlet is located at the upper left position, the methanol/water inlet is at the bottom left position. The flow direction is in each case crosswise. Higher air flow (right) leads to a significant temperature drop in the air inlet region due to water evaporation at the cathode, whereas the medium temperature increases due to heat generation.

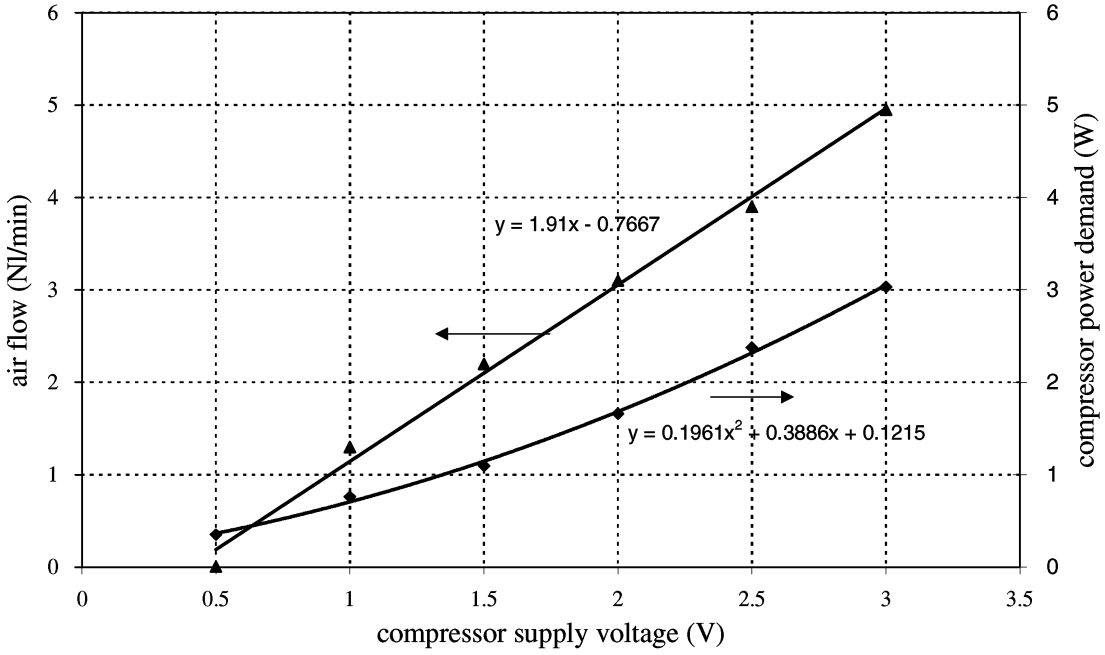

Fig. 8. Air flow and power demand of the compressor. The air pumped to the fuel cell is still on ambient pressure. The compressor is designed to create a maximum overpressure of 0.5 bar. At constant compressor power demand, this pressurization reduces the flow rate to half.

for different stack currents. The air inlet is located at the upper left side, the methanol inlet is at the bottom of the left side. The flow direction is crosswise. Increasing the current increases the air demand, with increasing cooling effects due to water evaporation at the cathode. At 15 A cell current, the temperature of the upper left quarter of the cell is approx. 5–8 °C lower than the rest. This effect could be reduced by a pre-humidification of the inlet air, which will be investigated in the future.

5.1. System issues

The system efficiency is a function of the efficiency of the fuel cell and the energy demand of the auxiliary components.

Defining

$$\eta_{\text{aux}} = \frac{P_{\text{fc}} - \sum P_{\text{aux}}}{P_{\text{fc}}}$$

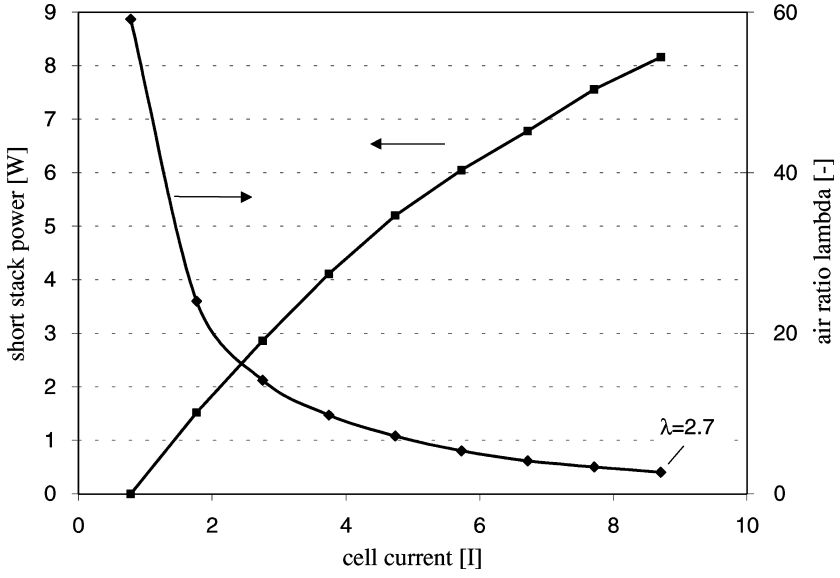

Fig. 9. Short stack power and air ratio vs. the cell current. As the compressor is connected directly to the fuel cell increasing cell current leads to a decrease of the flow rate and the air ratio. The short stack power is the net power, i.e. the generated power by the stack less the compressor power consumption.

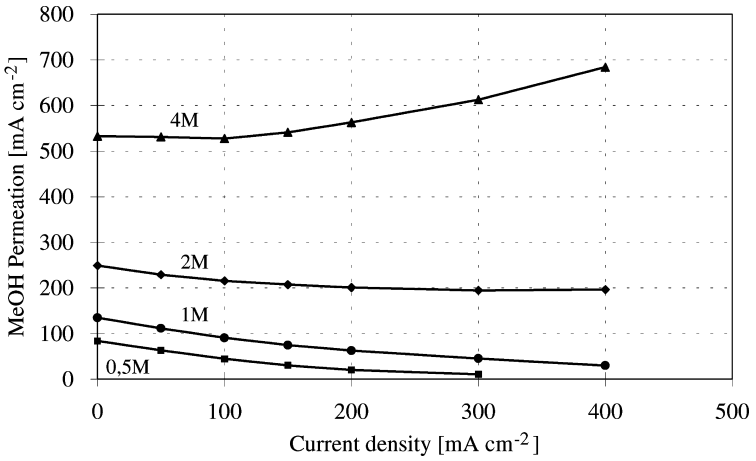

Fig. 10. Influence of the methanol concentration and the current density on the methanol permeation. The methanol permeation is expressed as a current density according to the law of Faraday. Single cell measurement; temperature, 110 °C; pressure, 3 bar.

as an efficiency of the auxiliary system components compared to the fuel cell power output P_{fc}. In addition defining

$$\eta_{system} = \frac{P_{fc} - \sum P_{aux}}{P_{fc}} \eta_{fc}$$

leads to an expression for the overall system efficiency, including the fuel cell and the auxiliary components. The fuel cell efficiency η_{fc} depends on the cell voltage and the fuel utilization.

To get information about the energy demand of the compressor and the minimum air flow rate of the fuel cell, we connected the compressor electrically in parallel to the fuel cell, as well as, to an additional electronic load. For these measurements, the 3-cell short stack was used within a voltage range from approx. 1 to 1.8 V. From separate experiments, the flow rates and the power demand of the compressor depending on the voltage were determined (Fig. 8). With decreasing voltage, the flow rate significantly drops down, i.e. the stoichiometric air ratio λ decreases rapidly to the minimum of $\lambda = 2.7$, at a cell current of 8.7 A (0.7 A compressor current, 8 A additional current) which is shown in Fig. 9.

Among the operation conditions, the methanol permeation has the strongest impact on the overall system efficiency. The methanol permeation from the anode to the cathode results in an additional methanol consumption lowering the fuel utilization, and lowering the cathode potential due to the formation of a mixed potential. By using appropriate low methanol concentrations, it is possible to increase the fuel utilization up to approx. 90%. In Fig. 10, the

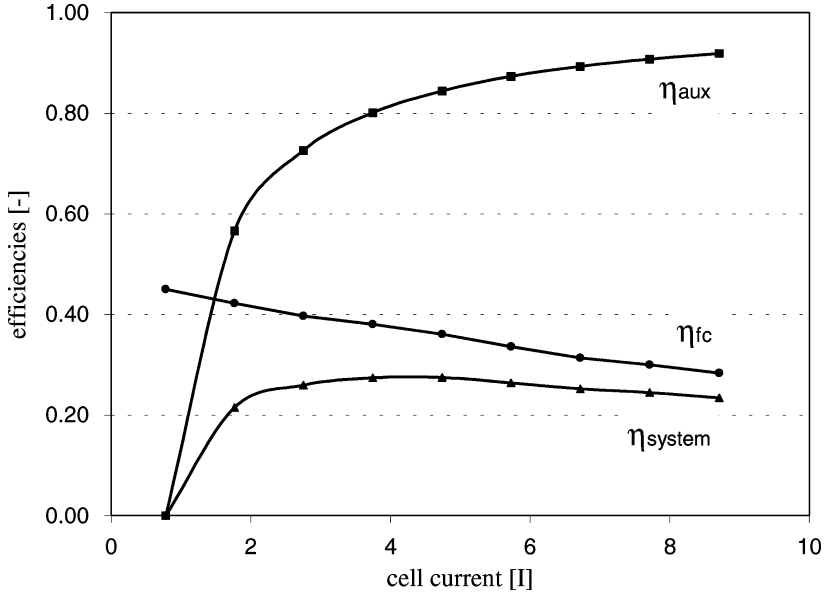

Fig. 11. System efficiency of the 3-cell short stack assembly with an air compressor connected to the stack. Fuel utilization is assumed to be 90% which is achievable for appropriate low methanol concentrations (see Fig. 10).

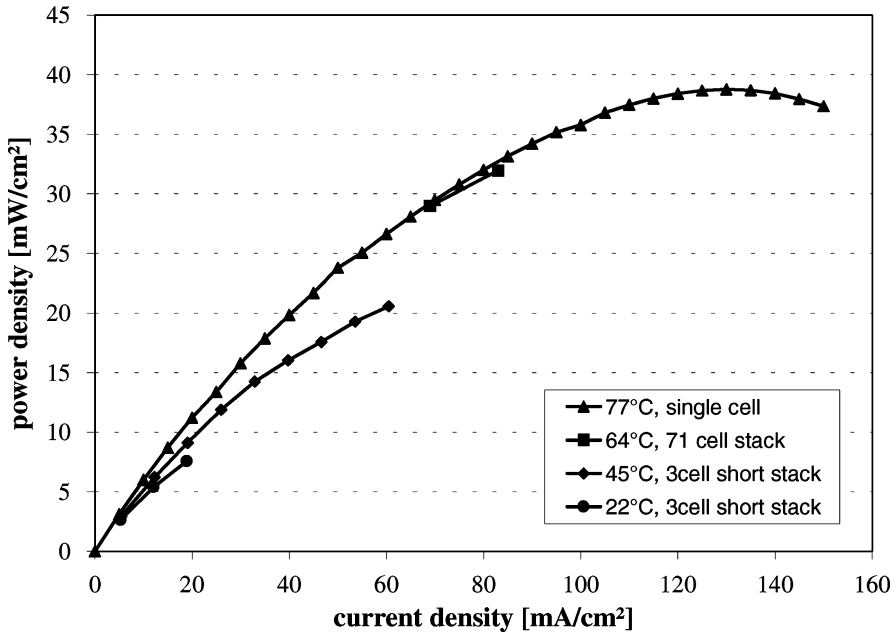

Fig. 12. Influence of the temperature on the power density of the DMFC with air at ambient pressure. Methanol concentration, 1 M.

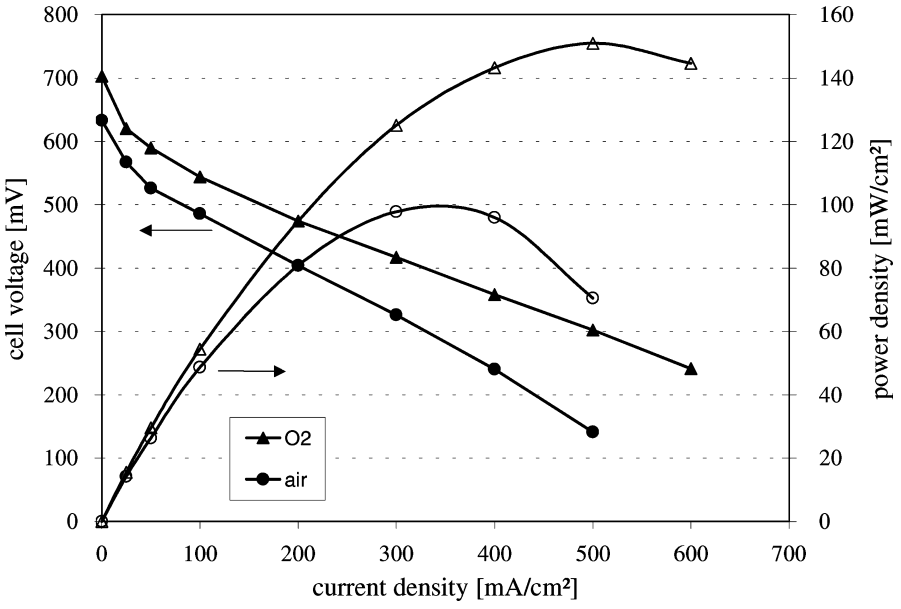

Fig. 13. Voltage/current density curves at elevated pressure (3 bar). Methanol concentration, 1 M; temperature, 80 °C. Data obtained from single cell measurements.

Table 2
Influence of the temperature on the cell performance[a]

T (°C)	i (mA/cm^2)	P (mW/cm^2)
22	18.9	7.6
45	39.8	16.0
64	76.0	30.4
77	80.0	32.0

[a] Operating conditions are ambient pressure; methanol concentration, 1 M; cell voltage, 400 mV.

methanol permeation is expressed as a parasitic current density for different methanol concentrations. On the other hand, the methanol concentration must be high enough to prevent a decrease of anode performance due to limiting current formation. With regard to the system efficiency, the careful adjustment of the methanol concentration is of utmost importance.

Assuming a fuel utilization of 90% for the 3-cell short stack, the system efficiency is in the range of 25–30%, as shown in Fig. 11.

5.2. Temperature

The effect of the temperature on the power at ambient pressure is shown in Fig. 12, and is summarized in Table 2. At elevated temperature (77 °C), the power is four times higher than under ambient conditions (22 °C). Due to evaporation of water at the cathode, the operating temperature is limited depending on the cathode pressure. Using air at ambient pressure, the temperature is limited to approx. 90 °C. Exceeding this temperature leads to an increase of the partial pressure of the water vapor, thus, decreasing the oxygen partial pressure towards limiting conditions.

6. Future work

Measurements to identify the optimal temperature and methanol concentration are going on at the moment. The power density of the stack can easily be increased by using an increased cathode pressure or by using oxygen. Fig. 13 finally shows voltage/current density curves at elevated pressure. The maximum power increases to 100 mW/cm^2 using air, and to 150 mW/cm^2 using oxygen at 3 bar absolute pressure. Operation at elevated pressures is an option, rather for transport applications, than for small portable power sources with the demand for simple and light weight system components.

References

[1] K. Kordesch, G. Simader, Fuel Cells and Their Applications, VCH, Weinheim, 1996.
[2] H. Dohle, Ph.D. thesis, RWTH Aachen, 2000.
[3] X. Ren, P. Zelenay, S. Thomas, J. Davey, S. Gottesfeld, J. Power Sources 86 (2000) 111.
[4] A. Havránek, K. Klafki, K. Wippermann, in: Proceedings of the 1st European Polymer Electrolyte Fuel Cell Forum, Luzern, Switzerland, 2–6 July 2001, submitted for publication.
[5] S. Gottesfeld, et al., in: Proceedings of the Electrochemical Society Meeting, Boston, 1998, p. 267.
[6] H. Dohle, J. Mergel, H. Scharmann, H. Schmitz, in: Meeting Abstracts of the 199th Meeting of the Electrochemical Society, Abstract no. 90, Washington, DC, 25–29 March 2001.
[7] T. Bewer, H. Dohle, T. Beckmann, J. Mergel, R. Neitzel, D. Stolten, in: Proceedings of the 1st European Polymer Electrolyte Fuel Cell Forum, Luzern, Switzerland, 2–6 July 2001, submitted for publication.